CHEMISTRY OF MATERIALS
Article

Chem. Mater. **2009,** *21,* 5237–5243 5237
DOI:10.1021/cm902231s

Formation of Hollow Upconversion Rare-Earth Fluoride Nanospheres: Nanoscale Kirkendall Effect During Ion Exchange

Fan Zhang,[†,‡] Yifeng Shi,[‡] Xiaohong Sun,[‡] Dongyuan Zhao,[†] and Galen D. Stucky*[,‡]

[†]*Department of Chemistry, and Laboratory of Advanced Materials, Fudan University, Shanghai 200433, P. R. China, and, and* [‡]*Department of Chemistry and Biochemistry, University of California Santa Barbara, California 93106-9510*

Received July 21, 2009. Revised Manuscript Received September 22, 2009

In this work, we report a facile solution-phase synthesis of hollow cubic phase α-$NaYF_4$ nanoparticles by a controlled ion exchange process from cubic phase Y_2O_3 nanospheres. We demonstrate that hollow nanoparticles with controlled size are formed owing to the nanoscale Kirkendall effect. The formation mechanism was studied with the XRD, STEM, and EDS line scanning characterization. The crystal structure similarity between the parent and the final product is essential for framework and morphology preservation. Although the sphere particles are polycrystalline and composed of the nanocrystals, the cubic structure of α-$NaYF_4$ nanocrystals displays a noticeable structure similarity with Y_2O_3, which we believe facilitates ion exchange between the primary nanocrystals and preservation of the secondary sphere morphology. The multicolor upconversion (UC) fluorescence (PL) was successfully realized in the $Yb^{3+}/Er^{3+}(Tm^{3+})$ codoped α-$NaYF_4$ hollow nanospheres by excitation in the near-infrared (NIR) region. The various UC emission ratios of the samples were investigated as a function of hydrothermal reaction time to research the UC properties of the products and to further demonstrate the thermodynamic driving solution ion-exchange process.

Introduction

Upconversion (UC) luminescent materials with anti-stokes optical property[1,2] have garnered considerable attention because of their potential applications as luminescence nanodevices including solid-state lasers,[3] flat-panel displays,[4] solar cells,[5] and optical-fiber-based telecommunications.[6] For biological applications, UC nanomaterials have many advantages over the conventional organic dye markers and quantum dots,[7,8] such as high chemical stability, low toxicity, high signal-to-noise ratio due to the absence of autofluorescence and high penetration depth in tissues. Until now, $NaYF_4$ has been found to be one of the most efficient hosts for visible UC fluorescence (PL),[9] and various nanostructures of $NaYF_4$ have been synthesized by different methods.[10−17] Fabrication of both cubic (α phase) and hexagonal (β phase) $NaYF_4$ has received considerable attention in recent years, and a number of methods have become available, including solid treatment,[1] coprecipitation in aqueous phase,[9,10] soft and hard template routes,[11,12] hydrothermal/solvothermal synthesis[13,14] and a surfactant controlled organometallic pyrolysis approach.[15−17] However, few studies have focused on the fabrication of the hollow spherical nanoparticles, which are more desirable for biolabels and drug-delivery applications. Hollow nanostructures can be readily synthesized by using the nanoscale Kirkendall effect.[18−21] Since the first report on the preparation of hollow CoS and CoO nanoparticles by sulfidation and oxidation of Co nanoparticles by exploitation of the Kirkendall effect,[18] a

*Corresponding author. E-mail: stucky@chem.ucsb.edu.

(1) Auzel, F. *Chem. Rev.* **2004**, *104*, 139–174.
(2) Wang, F.; Liu, X. G. *Chem. Soc. Rev.* **2009**, *38*, 976.
(3) Scheps, R. *Opt. Exp.* **2009**, *17*, 235–247.
(4) Downing, E.; Hesselink, L.; Ralston, J.; Macfarlane, R. A. *Science* **1996**, *273*, 1185–1189.
(5) Badescu, V. *J. Appl. Phys.* **2008**, *104*, 113120.
(6) Kaczmarek, F.; Stryla, Z.; Jendrzejczak, A. *Appl. Phys. B: Laser Opt.* **2001**, *73*, 125.
(7) Van, D.; Rijke, F.; Zijlmans, H.; Li, S.; Vail, T.; Raap, A. K. *Nat. Biotechnol.* **2001**, *19*, 273–276.
(8) Li, Z. Q.; Zhang, Y.; Jiang, S. *Adv. Mater.* **2008**, *20*, 1–5.
(9) Heer, S.; Kompe, K.; Gudel, H. U.; Haase, M. *Adv. Mater.* **2004**, *16*, 2102–2105.
(10) Yi, G. S.; Lu, H. C.; Zhao, S. Y.; Yue, G.; Yang, W. J. *Nano. Lett.* **2004**, *4*, 2191–2196.
(11) Zhang, F.; Wan, Y.; Shi, Y. F.; Tu, B.; Zhao, D. Y. *Chem. Mater.* **2008**, *20*, 3778.
(12) Zhang, F.; Zhao, D. Y. *Nano. Res.* **2009**, *2*, 292–305.
(13) Zhang, F.; Wan, Y.; Ying, T.; Zhang, F. Q.; Shi, Y. F.; Xie, S. H.; Li, Y. G.; Xu, L.; Tu, B.; Zhao, D. Y. *Angew. Chem., Int. Ed.* **2007**, *46*, 7976–7979.
(14) Zhuang, J. L.; Wang, J.; Yang, X. F.; Williams, I. D.; Zhang, W.; Zhang, Q. Y.; Feng, Z. M.; Yang, Z. M.; Liang, C. L.; Wu, M. M.; Su, Qiang *Chem. Mater.* **2009**, *21*, 160–168.
(15) Mai, H. X.; Zhang, Y. W.; Si, R.; Yan, Z. G.; Yan, C. H. *J. Am. Chem. Soc.* **2006**, *128*, 6426–6436.
(16) Boyer, J. C.; Vetrone, F.; Cuccia, L. A.; Capobianco, J. A. *J. Am. Chem. Soc.* **2006**, *128*, 7444–7445.
(17) Sivakumar, S.; van Veggel, F. C. J. M.; May, P. S. *J. Am. Chem. Soc.* **2007**, *129*, 620.
(18) Yin, Y. D.; Rioux, R. M.; Erdonmez, C. K.; Hughes, S.; Somorjai, G. A.; Alivisatos, A. P. *Science* **2004**, *304*, 711.
(19) Fan, H. J.; Gosele, U.; Zacharias, M. *Small* **2007**, *3*, 1660.
(20) Yin, Y. D.; Erdonmez, C. K.; Cabot, A.; Hughes, S.; Alivisatos, A. P. *Adv. Funct. Mater.* **2006**, *16*, 1389.
(21) Liang, X.; Wang, X.; Zhuang, Y.; Xu, B.; Kuang, S.; Li, Y. D. *J. Am. Chem. Soc.* **2008**, *130*, 2736.

Published on Web 10/12/2009

variety of hollow nanoparticles have been fabricated by a similar approach.[18−21] Most recently, an alternative ion exchange method has been used to alter the composition of the material by replacing the cations (anions) within the nanocrystal lattice with a different cation (anion).[22−26] In one example, the addition of Ag^+ to cadmium chalcogenide nanocrystals (CdS, CdSe, CdTe) led to their complete conversion to the corresponding silver chalcogenide.[22] In another, we demonstrated the production of β-$NaMF_4$ nanotubes through a hydrothermal in situ ion exchange reaction by using $M(OH)_3$ as precursor.[24] The structure similarity was found to be a requirement for the reaction. Remarkably, the morphology of anisotropic nanocrystals was preserved after ion exchange.[26]

Here we report a facile solution-phase synthesis of hollow cubic phase α-$NaYF_4$ nanoparticles by a controlled ion exchange process from cubic phase Y_2O_3 nanospheres. We demonstrate that hollow nanoparticles with controlled size are formed owing to the nanoscale Kirkendall effect. Multicolor UC PL is observed in the Yb^{3+}/Er^{3+} (green) and Yb^{3+}/Tm^{3+} (blue) codoped $NaYF_4$ nanospheres by excitation in the near-infrared (NIR) region.

Experimental Section

Homogeneous Precipitation Synthesis of Y_2O_3 Nanosphere. The $Y(OH)CO_3 \cdot H_2O$ precursor was first synthesized by a homogeneous precipitation method. In a typical synthesis, 6 mL of 1.0 M $Y(NO_3)_3$ and 12 g of urea were dissolved in 400 mL of H_2O with continuous stirring for 20 min. Then the mixture was sealed in a glass bottle and heated to 90 °C for 2 h. The resulting dispersions were centrifuged at 5000 rpm for 5 min, the supernatant solution was discarded, and the particles were resuspended in ethanol with an ultrasonic bath. This process was repeated three times, and then the precursor was dried and stored in a desiccator.

Y_2O_3 was obtained by thermal treatment of the precursor at 500 °C for 3 h (2 °C/min to 500 °C), the morphology was retained after the heat treatment.

The detailed reaction processes for the $Y(OH)CO_3 \cdot H_2O$ precursor formation through homogeneous precipitation are listed below:

$$H_2N{-}CO{-}NH_2 \rightarrow NH_4^+ + OCN^-$$

$$OCN^- + OH^- + H_2O \rightarrow NH_3 + CO_3^{2-}$$

Yttrium ions are weakly hydrolyzed in water to $YOH(H_2O)_n^{2+}$

$$YOH(H_2O)_n^{2+} + CO_2 + H_2O \rightarrow YOHCO_3 \cdot H_2O + 2H^+ + (n-1)H_2O$$

Synthesis of Rare Earth Fluoride Hollow Nanosphere. In a typical synthesis, 0.1 g of NaF and 3 mL of 0.1 M HF were dissolved in 8 mL of deionized water with stirring for 5 min, then 0.75 g of Y_2O_3 nanospheres prepared as the above was added into the mixture solution. After 5 min stirring, the mixture solution was transferred into a stainless-steel autoclave and heated at 100 °C for 3 h. After cooling, the powder sample was washed with deionized water and ethanol for several times and dried at in a desiccator overnight. (The hazards of using HF are described in the Supporting Information.)

Synthesis of Lanthanide-Doped Rare Earth Fluoride Hollow Nanosphere. The preparation of the lanthanide-doped rare-earth fluoride nanospheres was similar to the above procedure. For example, to prepare α-$NaYF_4$ doped with 20 wt % Yb^{3+} and 2 wt % Er^{3+}, 5.28 mL of 1.0 M $Y(NO_3)_3$, 2.1 mL of 0.63 M $Yb(NO_3)_3$ and 0.3 mL of 0.40 M $Er(NO_3)_3$ were mixed together to replace 6 mL of 1.0 M $Y(NO_3)_3$. After homogeneous reaction at 90 °C for 2 h in the presence of 12 g of urea and 400 mL of H_2O, the (Y, Yb, Er)$OHCO_3 \cdot H_2O$ could be obtained. The Y_2O_3 doped with 20 wt % Yb^{3+} and 2 wt % Er^{3+} was obtained by thermal treatment of the precursor at 500 °C for 3 h (2 °C/min to 500 °C). The α-$NaYF_4$:20 wt % Yb^{3+}, 2 wt % Er^{3+} could be obtained with Y_2O_3:20 wt % Yb^{3+}, 2 wt % Er^{3+} as a parent in the presence of NaF and HF through the ion exchange process.

Characterization. X-ray diffraction (XRD) patterns were collected on a Scintag PADX diffractometer with Cu Kα radiation (45 kV, 35 mA). Transmission electron microscopy (TEM) images were taken using a FEI Tecnai T20 Sphera electron microscope operating at 200 keV. FEI Titan 300 kV FEG TEM/STEM System w/EDS and EELS was used to take the STEM image and EDS line scanning. Scanning electron microscopy (SEM) images were acquired on a FEI XL30 Sirion FEG digital scanning electron microscope. Nitrogen sorption isotherms were measured at 77 K on a Micromeritics Tristar 3000 analyzer (USA).

UC PL measurements were done on a homemade PL spectrometer. Excitation light with wavelength 970−980 nm was generated by a continuous wave (CW) Ti:Sapphire laser (Spectraphysics 3900S) pumped by an Ar^+-laser (Spectraphysics Beamlock 2060). The near-infrared (NIR) laser output passed through a long wavelength-pass filter (Newport LP830) to remove visible and NIR PL of the Ti:Sapphire crystal and neutral density filter wheel which was used to adjust the excitation beam power. The laser beam was focused on the sample by a lens with long focal distance of 15 cm. The UC PL was collected at 45° by a two-lens system and focused on the entrance slit of a spectrograph (Acton Research SpectraPro-500). NIR light scattered by the sample was blocked by a short wavelength-pass filter (Newport KG3). The luminescence was dispersed by the spectrograph and detected by a TE-cooled CCD camera (Roper Scientific PIXIS-400). The water adsorbed on the upconverison cannot be excluded especially in the hydrothermal reaction conditions. But in our case, to investigate the upconversion properties in the water solution of hydrophilic α-$NaYF_4$ nanospheres, which are desired by the biological applications, the upconversion tests were conducted in the water solutions. Therefore, we think the effect of water on the emission should be same for all the samples during the ion exchange process.

Results and Discussion

Monodispersed $Y(OH)CO_3 \cdot H_2O$ nanosphere precursor particles (Figure 1A) can be prepared via a homogeneous precipitation method from an aqueous solution of yttrium nitrate and urea at 90 °C for 2 h.[27]

(22) Son, D. H.; Hughes, S.; Yin, Y. D.; Alivisatos, A. P. *Science* **2004**, *306*, 1009.
(23) Camargo, P. H. C.; Lee, Y. H.; Jeong, U.; Zou, Z. Q.; Xia, Y. N. *Langmuir*. **2007**, *23*, 2985–2992.
(24) Wark, S. E.; Hsia, C. H.; Son, D. H. *J. Am. Chem. Soc*. **2008**, *130*, 9550–9555.
(25) Sadtle, B.; Demchenko, D. O.; Zheng, H. M.; Hughes, S. M.; Merkle, M. G.; Dahmen, U.; Wang, L. W.; Alivisatos, A. P. *J. Am. Chem. Soc*. **2008**, *131*, 5285–5293.
(26) Zhang, F.; Zhao, D. Y. *ACS Nano* **2009**, *3*, 159.
(27) Aiken, B.; Hsu, W. P.; Matijevic, E. *J. Am. Ceram. Soc*. **1988**, *71*, 845.

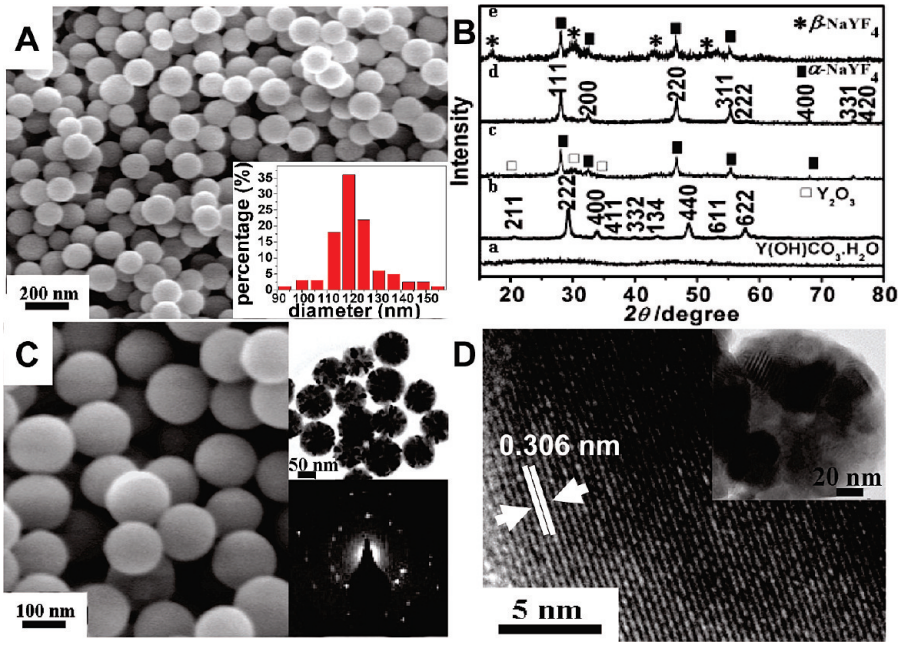

Figure 1. (A) SEM image of $Y(OH)CO_3 \cdot H_2O$ nanospheres, (inset) the particle size distribution of the nanospheres dispersed in the water solution; (B) XRD patterns of the $Y(OH)CO_3 \cdot H_2O$ (a), Y_2O_3 (b), Y_2O_3/α-$NaYF_4$ composite after 1 h reaction (c), pure α-$NaYF_4$ after 3 h reaction (d), and α-$NaYF_4$/β-$NaYF_4$ composite after 4 h reaction (e); (C) SEM image of Y_2O_3 nanospheres; (inset) the TEM image of Y_2O_3 nanospheres and SAED pattern recorded on a single spherical particle; (D) HRTEM images of the Y_2O_3 nanocrystal composed in the nanospheres; (inset) a high-magnification TEM image of Y_2O_3, showing the primary small nanocrystals making up the nanosphere.

The formation mechanism of the nanospheres can be understood as a two-stage growth model, in which nanosized amorphous precursors are nucleated first in supersaturated solution and then the small particles initially formed assemble into larger secondary particles. SEM images of as-synthesized $Y(OH)CO_3 \cdot H_2O$ precursor show uniform solid spheres with smooth surfaces and diameters of ~120 ± 5 nm (Figure 1A and inset). XRD results reveal that the precursor particles are amorphous (Figure 1B-a). After thermal treatment at 550 °C for 3 h, the cubic phase Y_2O_3 (space group *Ia*3 (No. 206)) with lattice constant a = 10.50 Å is obtained. The broadening of the diffraction peaks confirms that monodispersed Y_2O_3 nanospheres are composed of the primary small particles (3−20 nm) (Figure 1B-b). SEM image shows that there is no obvious change of the morphology and size after the heat treatment (Figure 1C). TEM images show that each solid nanosphere is composed of many small nanocrystals, with a size distribution of about 5−15 nm (Figure 1C inset). SAED patterns recorded from a single sphere confirm that the Y_2O_3 nanosphere is polycrystalline (Figure 1C inset). HRTEM results based on the crystal fringes reveal that the distances between the adjacent crystal fringes have the same value, 0.306 nm, which can be assigned to the {222} crystal plane of the Y_2O_3 bcc phase (Figure 1D). The specific surface areas have been confirmed to be 23.8 m^2/g by BET measurement. This result also supports that the secondary structures of the Y_2O_3 nanosphere for the measured specific surface areas are much higher than the calculated value for the single-crystal with identical size (7.3 m^2/g).

The α-$NaYF_4$ hollow sphere nanoparticles can be prepared via the ion-exchange reaction of Y_2O_3 nanospheres in the presence of HF and NaF solution with the hydrothermal method at 100 °C for 3 h. SEM images show that the samples are well-preserved uniform nanospheres (Figure 2A,B). In contrast to the Y_2O_3 nanosphere parents, the α-$NaYF_4$ nanospheres have a slightly larger diameter of 125 ± 5 nm (Figure 2A inset), and exhibit rather rougher surfaces. Their hollow structure can be clearly observed on examination of broken particles (Figure 2B). TEM images reveal that the hollow nanospheres have a shell consisting of interconnected, irregularly shaped nanocrystals with an average size of 8 nm, which results in an average shell thickness of about 30 nm (Figure 2C). SAED patterns recorded on a single sphere show that the α-$NaYF_4$ is polycrystalline (Figure 2D, inset). HRTEM images clearly reveal that there are two different set atomic lattice fringes in the same domain, as expected for the {111} and {220} crystal planes of α-$NaYF_4$ cubic phase (Figure 2D), further confirming the polycrystalline property of the product. XRD patterns of hollow nanospheres can be assigned to the pure cubic phase $NaYF_4$ with a lattice parameter of a = 5.47 Å (JCPDS 77-2042; $Fm\bar{3}m$). No obvious reflections of Y_2O_3 were found, confirming a complete transformation (Figure 1B-d). EDS line scans across the hollow nanosphere reveal that the composition of this product is Na/Y/F. No oxygen was detected, confirming a complete transformation (Figure 2E). The material has high specific surface area (162.3 m^2/g), large pore volume (2.25 cm^3/g), and average pore size of 3.8 nm that are expected to serve as a carrier for drug delivery.

To understand the formation mechanism of the α-$NaYF_4$ hollow sphere nanoparticles, we carried out

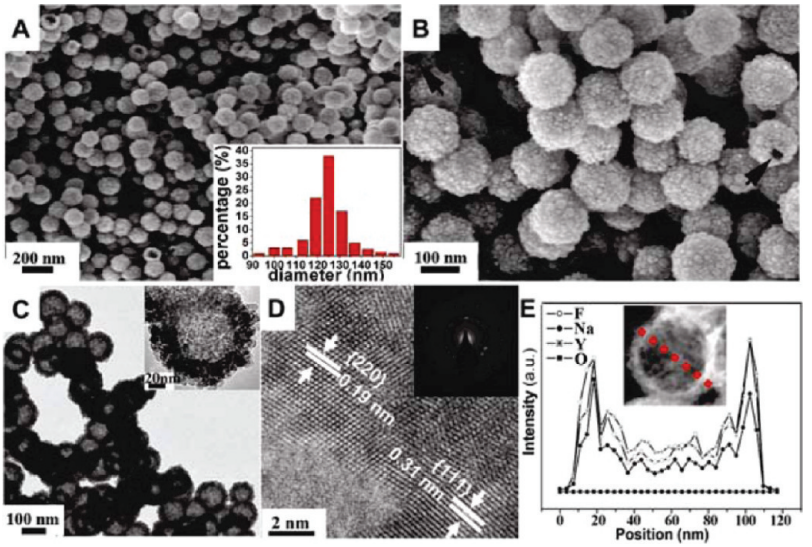

Figure 2. SEM images of α-$NaYF_4$ hollow nanospheres (A,B); (inset in A) the particle size distribution of the hollow nanospheres dispersed in the water solution. (C) TEM image of α-$NaYF_4$ hollow nanospheres; (inset) high-magnification TEM image of a single particle. (D) HRTEM image of the α-$NaYF_4$ nanocrystals composed in the nanospheres; (inset) SAED image of α-$NaYF_4$. (E) Compositional line profile across the hollow nanosphere by EDS line scanning; (inset) dark field STEM image of a single α-$NaYF_4$ nanoparticle. The red line is the EDS line scanning route (line scanning image is the normalized figure).

step-dependent experiments. XRD patterns reveal that the samples are Y_2O_3/α-$NaYF_4$ composites after 1−2 h reaction (Supporting Information, Figure S1). Morphology evolution as a function of reaction time at 100 °C reveals that small voids can be observed between the core and shell after 1 h (Figure 3A). An obvious gap between the core and shell developed after 1.5 h, and the bulk core in the hollow interior could be clearly observed (Figure 3B). The core and shell can be seen to be connected by filament-like bridges, resembling structures reported previously.[20] These bridges might act as fast-transport paths for the delivery of the remaining Y_2O_3 to the shell.[20] The compositional line profile across a single hollow core−shell structure probed by EDS line scanning reveals that the F content in the fringe area is much higher than that in the center area, which confirms that the shell structure is α-$NaYF_4$ and the core material is unconsumed Y_2O_3 (Figure 3F). The core disappears slowly and a single void with some remaining filament nearby the shell is observed after 2 h (Figure 3C). EDS line scanning reveal that there are still some oxygen atoms on the edge (Figure 3G). These remaining oxygen atoms disappear as the reaction proceeds to completion, leading to hollow nanospheres with distinguishable, regular, well-centered circular voids after 3 h (Figure 3D,H). XRD results show that pure phase α-$NaYF_4$ is obtained after a 3 h treatment. We found that solid α-$NaYF_4$ nanospheres could also be obtained at 80 or 100 °C after 3 h with continuous stirring (Supporting Information Figure S2a). Some α-$NaYF_4$ hollow nanospheres were observed when the reaction proceeded at 80 °C for 3 h without stirring (Figure S2b), and only hollow nanospheres were observed at 100 °C without stirring (Figure 2A). We believe that stirring increases the inward diffusion rate of F^- allowing ion exchange in a homogeneous medium, which realizes solid nanosphere formation.

According to our previous research,[26] the crystal structure similarity between the parent and the final product is essential for framework and morphology preservation. In that regard, although the sphere particles are polycrystalline and composed of the nanocrystals, the cubic structure of α-$NaYF_4$ nanocrystals display a noticeable structure similarity with Y_2O_3, which could facilitate ion exchange between the primary nanocrystals and preservation of the secondary sphere morphology. However, the reaction conditions must be controlled in order to maintain the cubic phase α-$NaYF_4$. If the temperature and reaction time increase, the thermodynamic driving force can lead to a phase transformation from the metastable cubic phase to the more stable hexagonal phase. This results in the α-$NaYF_4$ nanocrystals reorganizing to form the large β-$NaYF_4$ single crystal particles (Supporting Information Figure S3). The hexagonal phase emerged after 4 h at 100 °C, when some rodlike single crystal nanoparticles could be observed (Figure 1B-e and Supporting Information Figure S4). When the temperature was increased to 130 °C (Figure S4), the hexagonal phase was formed after 1 h (Figure S4 and S5), and pure β-$NaYF_4$ could be formed after 6 h (Figure S4). Recently, Wu et al. reported the β-$NaYF_4$ synthesis with Y_2O_3 using the solvothermal method.[14] The Y_2O_3 prepared in their work also comprised a lot primary nanoparticles, but these primary nanoparticles (~30 to 200 nm) are larger in size than those obtained in our methods (3−20 nm). We think the smaller primary nanoparticle size in our work is one of the reasons for the ion exchange process from Y_2O_3 to α-$NaYF_4$ at low temperature (100 °C). Furthermore, and most importantly, we used the HF during the ion exchange process. In our experiment, the α-$NaYF_4$ cannot be obtained if we just use the NaF when the temperature is below 160 °C. When the temperature was increased to 160 °C, the Y_2O_3/β-$NaYF_4$

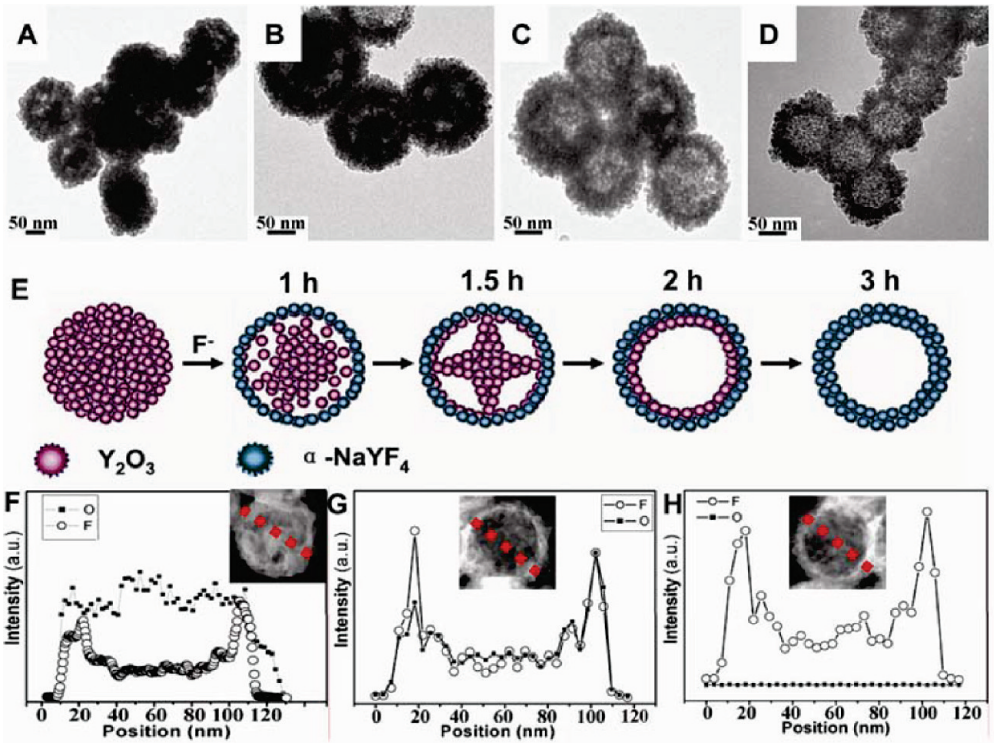

Figure 3. TEM images of samples obtained with different reaction times: 1 (A), 1.5 (B), 2 (C), and 3 h (D). Illustration of the α-$NaYF_4$ hollow nanospheres formation process based on the Kirkendall effect (E). Compositional line profile across the hollow nanosphere obtained at 1.5 (F), 2 (G) and 3 h (H). The inset is the dark field STEM image of a single nanosphere. The red line is the EDS line scanning route.

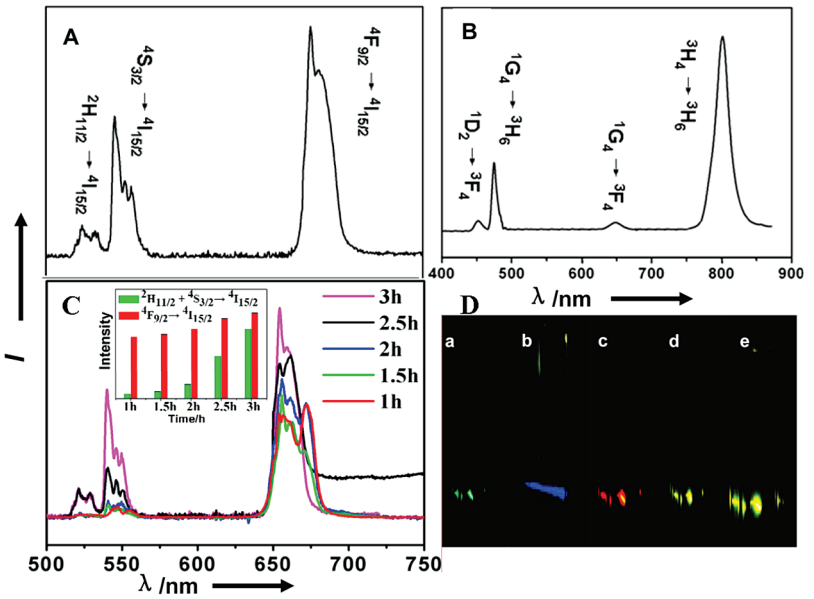

Figure 4. Spectroscopic characterization for UC luminescence. UC luminescence spectra of α-$NaYF_4$:2% Er^{3+}, 20% Yb^{3+} (A), α-$NaYF_4$:2% Tm^{3+}, 20% Yb^{3+} (B), excited with a 978 nm laser diode and samples as a function of the reaction time at 100 °C (C); the inset is the integrated green and red UC emission intensity as a function of the reaction time. (D) Photographs of the UC luminescence in 1 wt % water solution of α-$NaYF_4$:2% Er^{3+}, 20% Yb^{3+} (a), α-$NaYF_4$:2% Tm^{3+}, 20% Yb^{3+} (b), and samples as a function of the reaction time at 100 °C, 1 (c), 2 (d), and 2.5 h (e).

composite could be obtained only with the NaF (Supporting Information Figure S6).

These results indicate that the formation of α-$NaYF_4$ hollow nanospheres can be explained through a fundamental solid-state phenomenon, the Kirkendall effect, which deals with the movement of the interface between diffusion couples. The secondary structures of the Y_2O_3 give the nanosphere high reactivity and diffusion rates for F^- ion exchange.[20] Furthermore, the diffusion rates associated with the Y_2O_3 nanosphere secondary nanostructure made up from the Y_2O_3 primary nanocrystals are obviously much faster than that of the Y_2O_3 single-crystal nanostructure.[26] If the calcination temperature for the Y_2O_3 is increased above 600 °C, the nanocrystals composed in the nanosphere sinter to form larger nanoparticles, and the secondary structure disappears

gradually as the heat treatment increases. As a result, it is difficult to obtain hollow nanospheres through the ion exchange process with F substitution (Supporting Information Figure S7).

XRD patterns reveal that pure α-$NaYF_4$:Yb, Er/Tm samples can be obtained with Y_2O_3:Yb, Er/Tm nanospheres as precursors (Supporting Information Figure S8). SEM and TEM images (Supporting Information Figure S9) show that the α-$NaYF_4$:2% Er^{3+}, 20% Yb^{3+} and α-$NaYF_4$:2% Tm^{3+}, 20% Yb^{3+} nanospheres with uniform shape and size can be synthesized with the hydrothermal ion exchange process. These results suggest that the doped ions have little effect on the morphology and size.

Multicolor UC PL spectra are observed in the Yb^{3+}/Er^{3+}(green) and Yb^{3+}/Tm^{3+}(blue) codoped α-$NaYF_4$ hollow nanospheres. The visible and NIR UC luminescence spectra of α-$NaYF_4$:2% Er^{3+}, 20% Yb^{3+}, and α-NaYF4:2% Tm^{3+}, 20% Yb^{3+} under infrared excitation (978 nm) are shown in Figure 4 panels A and B, respectively. The emission bands are assigned to transitions within the 4f−4f levels of Er^{3+} and Tm^{3+} ions (Figure 5). In the Yb^{3+}/Er^{3+} codoped α-$NaYF_4$ sample, green luminescence between 510 and 570 nm can be assigned to the ($^2H_{11/2}$, $^4S_{3/2}$) → $^4I_{15/2}$ transition. A red emission is observed between 630 and 680 nm originating from the $^4F_{9/2}$ → $^4I_{15/2}$ transition. In the case of Tm^{3+}, the visible luminescence originates from two stages: $^1G_4$ → $^3H_6$ and $^1D_2$ → $^3F_4$. The former results in a blue emission between 450 and 490 nm, and the latter yields a weak red emission between 630 and 680 nm. Furthermore, an intense NIR emission can be observed between 750 and 850 nm due to the $^3H_4$ → $^3H_6$ transition (Supporting Information Figure S10).

The UC emission intensities and the ratios of the various emissions are influenced by the doping levels, excitation power, preparation temperature, and impurities.[1,26,28] In particular, the oxygen effect is very important for the UC emission efficiency. The relative emission intensities of the two constituent colors can be changed so that it is possible to tune the color output of the hollow nanospheres as the emission changes significantly with time during the hydrothermal ion exchange reaction at 100 °C (Figure 4C). The intensity of the red UC luminescence at 650 nm is always stronger than that of the green at 540 nm, and the ratio of the red to green decreases gradually as the reaction time increases from 1 to 3 h, which can be ascribed to the oxygen effect.[26,28,29] For the Yb^{3+}/Er^{3+} (green) codoped β-$NaYF_4$ hollow nanosphere, oxygen can increase the multiphonon relaxation rates between the metastable states, which reduces the overall visible emission intensity and enhances the red to green emission ratios as previously reported.[26,28−31] The

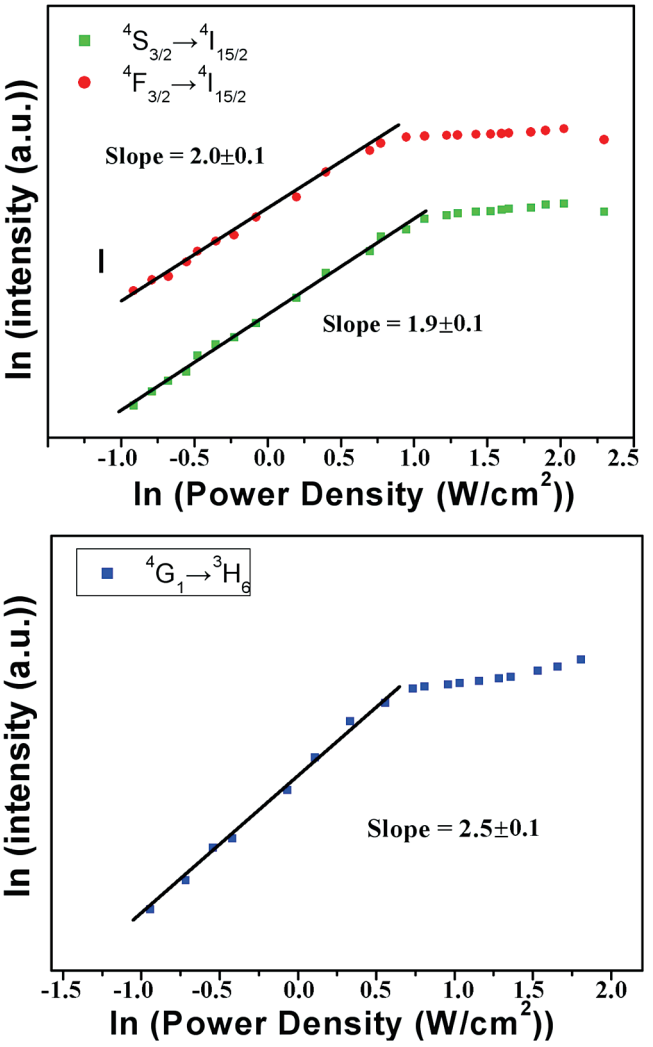

Figure 5. Power dependence of the upcoverted emissions of α-$NaYF_4$:2% Er^{3+}, 20% Yb^{3+} (A), α-$NaYF_4$:2% Tm^{3+}, 20% Yb^{3+} (B) excited with a 978 nm laser diode. For the α-$NaYF_4$:2% Er^{3+}, 20% Yb^{3+}, both the slopes for the red and green curves are about 2 at relatively low excitation densities, indicating a two-photon emission process. At high excitation density the slope of the curve is reduced because of saturation of the UC process. For the α-$NaYF_4$:2% Tm^{3+}, 20% Yb^{3+} sample, the slope for the blue emission curve is 2.5 at relatively low excitation densities, at high excitation density, the slope of the curve is reduced due to the saturation of the UC process.

UC luminescence of rare-earth ions mainly originates from the electron transitions within the 4f shell, which is highly sensitive to the composition and structure of the host materials.[1] Since the fluorescent transitions of rare-earth ions of practical importance are initiated from an excited level with a small energy gap, materials with lower phonon energy are required as the luminescent host to minimize nonradiative loss.[32] This is very important for the UC processes, because these are very sensitive to quenching by high-energy vibrations according to the energy-gap law.[33] The oxygen-based systems often have large phonon energy as a result of the stretching vibrations of the host molecules. In comparison, fluorides have

(28) Kramer, K. W.; Biner, D.; Frei, G.; Gudel, H. U.; Hehlen, M. P.; Luthi, S. R. *Chem. Mater.* **2004**, *16*, 1244–1251.
(29) Zhang, J. S.; Qin, W. P.; Zhao, D.; Hu, D. G. J.; Zhang, J. H.; Wang, Y.; Cao, C. Y. *J. Lumin.* **2007**, *122*, 506–508.
(30) Sivakumar, S.; van Veggel, F. J. M.; Stanley, P. *J. Am. Chem. Soc.* **2007**, *129*, 620–625.
(31) Wang, F.; Liu, X. G. *J. Am. Chem. Soc.* **2007**, *129*, 620–625.
(32) Yan, R. X.; Li, Y. D. *Adv. Func. Mater.* **2005**, *15*, 763.
(33) Klink, S. I.; Hebbink, G. A.; Grave, L.; Van Veggel, F. C. J. M.; Reinhoudt, D. N. R.; Slooff, L. H.; Polman, A.; Hofstraat, J. W. *J. Appl. Phys.* **1999**, *86*, 1181.

an advantage as a fluorescent host matrix due to their low vibrational energies,[34] and the subsequent minimization of the quenching of the excited state of the rare-earth ions. During the ion exchange process, the intermediate products are composed of two distinct phases of cubic Y_2O_3:Yb/Er and cubic $NaYF_4$:Yb/Er. As a result, the emission spectrum is actually a sum of emissions from dopants in both phases.

For Y_2O_3:Yb/Er, the ratio of the intensity of red emission to that of green emission is higher than that for $NaYF_4$:Yb/Er due to the energy-transfer (ET) process from Yb^{3+} to Er^{3+}.[35] Furthermore, the integrated emission intensity of Y_2O_3:Yb/Er is weaker than that of $NaYF_4$:Yb/Er. As a result, the integrated emission intensity and the green to red emission ratio will be increased with the reaction time increasing during the ion exchange process.

Photographs of eye-visible UC luminescence in water solutions of α-$NaYF_4$:2% Er^{3+}, 20% Yb^{3+} (Figure 4D-a) and α-$NaYF_4$:2% Tm^{3+}, 20% Yb^{3+} (Figure 4D-b) excited with a laser at 978 nm indicate that the α-$NaYF_4$ nanospheres are excellent UC hosts. Figures 4D-c,d,e show that the tunable color output of the hollow nanospheres from red to yellow green can be observed during the reaction time from 1 to 2.5 h. The power dependence of the green and red luminescence (Figure 5) was found to be approximately 2, indicating that two photons are involved in the UC mechanism.[1,2,26]

(34) Bender, C. M.; Burlitch, J. M.; Barber, D.; Pollock, C. *Chem. Mater.* **2008**, *20*, 3778.
(35) Matsuura, D.; Hattori, H.; Takano, A. *J. Electrochem. Soc.* **2005**, *152*, H39.

Conclusion

A successful synthesis of uniform α-$NaYF_4$ hollow nanospheres via hydrothermal ion exchange reaction by using Y_2O_3 solid nanospheres as a template is reported. It is demonstrated that hollow nanoparticles with retained morphology and size are formed due to the nanoscale Kirkendall effect. The polycrystalline α-$NaYF_4$ hollow nanospheres with uniform diameter (~125 nm) and wall thickness (~30 nm) are easily obtained. The thermodynamic driving force is a key to the formation of α-$NaYF_4$ via the hydrothermal ion-exchange approach. The crystal structural similarities (cubic phase) are essential to realize the ion exchange transformation. The multicolor UC PL was successfully realized in the $Yb^{3+}/Er^{3+}(Tm^{3+})$ co-doped α-$NaYF_4$ hollow nanospheres by excitation in the NIR region. The red to green emission ratio decreases as the oxygen decrease during the F-substituted process. It is expected that these rare earth fluoride hollow nanospheres might have potential in applications as building blocks for functional devices particularly for biolabel and drug-delivery applications.

Acknowledgment. The work was supported by the National Science Foundation under award No. DMR 08-05148.

Supporting Information Available: Experimental procedures, additional analysis of the Y_2O_3 and α-$NaYF_4$ prepared at different reaction conditions, and schematic energy level diagrams of the Er^{3+}, Tm^{3+}, and Yb^{3+} dopant ions and UC mechanism. This material is available free of charge via the Internet at http://pubs.acs.org.